Proceedings of the Canadian Society for Mechanical Engineering International Congress
32nd Annual Conference of the Computational Fluid Dynamics Society of Canada
Canadian Society of Rheology Symposium
CSME-CFDSC-CSR 2025
May 25–28, 2025, Montréal, Québec, Canada

ALL-WHEEL STEERING AND DRIVING CONTROL OF AN 8X8 SCALED ELECTRIC COMBAT VEHICLE

Michael Peiris[1*], Moustafa El-Gindy[1], Haoxiang Lang[1]
[1]Faculty of Engineering and Applied Science, Ontario Tech University, Oshawa, Canada
*michael.peiris@ontariotechu.net

Abstract— This investigation involves the steering and variable wheel speed control for an 8x8 scaled electric combat vehicle (SECV). The SECV was previously constructed at Ontario Tech University and is capable of steering all eight of its wheels to unique steering angles and applying independent variable wheel speeds to each of its eight wheels. The Ackermann steering geometry is used as the basis for the control of the vehicle. The Ackermann condition explains that during a turn, the wheels along an axle require different steering angles, tracing circular paths of differing radii to avoid additional lateral wheel scrubbing and wear. The control of both the steering angles and wheel speed of all eight wheels is performed in real time on the physical vehicle. In addition, three separate steering configurations are developed: traditional steering, fixed third axle steering and all wheel steering. The output steering angles, and output wheel speeds are evaluated while the vehicle is stationary with results for the all-wheel steering scenario presented. The main contribution of this research is the physical implementation and accurate control of the Ackermann condition for driving and steering control of the SECV prior to using the same control method for autonomous navigation.

Ackermann, multi-wheel vehicle, steering control, driving control, vehicles, robots

I. INTRODUCTION

In recent years, there have been many advancements in the areas of accurate steering and velocity control of vehicles. Current consumer vehicles are outfitted with various control systems to enhance safety of occupants including anti-lock braking [1] and traction control systems [2] as many manufacturers continue to add autonomous features [3]. In 2019 Wei et al. researched a vehicle-following control system that relied on vehicle-to-vehicle communication to predict and control the path of a second follower vehicle based on a controlled preceding vehicle [4]. This is also known as autonomous platooning where a lead vehicle being either autonomously or human operated navigates with one or several vehicles traveling immediately behind the lead vehicle. The motion of the follower vehicles is dependent on input received from the lead vehicle with the control system ensuring safe navigation though accurate spacing and speed of the following vehicles. In addition, the follower vehicles receive no human input or intervention. The authors of this study relied solely on a radar sensor for each follower vehicle and the historical motion data of the lead vehicle. It was seen that their proposed control method utilizes minimal sensors in the follower vehicles and shows reliable longitudinal and lateral performance. Furthermore, the system has no reliance on road markings and lane positioning.

Another interesting vehicle control method is seen by Lenzo et al. in 2020 where the authors attempted to control the sideslip and yaw rate angles of a vehicle in simulation and through experimentation [5]. The authors developed a single input, single output controller for the yaw rate with correction occurring based on the real time side slip angle. The system is validated through a simulated model as well as through physical experiments. The results show that the designed controller constrains the sideslip angle within predetermined allowable thresholds. Furthermore, physical experimentation is conducted with the ICOMPOSE prototype electric vehicle, outfitted with several sensors including a radar scanner and yaw rate sensor.

In terms of consumer vehicles, many platforms are able to provide additional information to the occupants through automated systems such as GPS positioning [6], blind spot detection [7], lane departure warning and automated braking. The current state of the art in this research field is focused on developing software and hardware systems to progress towards full autonomous navigation. However as seen in recent literature, the vast majority of studies involve developing and testing autonomous control methods purely in simulation. Furthermore, if experimentation is undertaken it is seen that the majority of experimental platforms or test vehicles leveraged lack car-like features seen in traditional automobiles such as suspension or actuated steering. Instead, many research studies use differential drive [8], also known as “skid steering” [9] to navigate. In the real world, this results in excessive tire wear during steering for the vehicle and is not desirable.

Another work in this area involving path following through rear axle steering control for a realistic vehicle is seen by Ahmed et al in 2021 [10]. This study is purely performed in simulation however the authors leverage a 22 degree of freedom vehicle model using Trucksim software. A unique benefit of this simulated study is that the vehicle model is complex and

composed of eight wheels, all capable of steering and the design is inspired by a military troop-carrying vehicle. The authors designed several rear axle controllers to actively steer the rear wheels of the vehicle to maintain its path and reduce tracking error. The controllers are evaluated alongside the virtual model through several high speed and low speed driving maneuvers. The results showed that the controller applied to the wheels on all axles had the best performance with the least lateral error. Further studies involving steering and driving control for military and other heavy vehicles can be seen by Ahmed et al. in 2020 [11] and 2021 [12]. Both studies use the same military vehicle model with all analysis performed in simulation using a Trucksim model.

In order to expand the research in the area of Ackermann controlled vehicles, it is the focus of this work to present the designed steering and velocity control systems for an eight-wheel drive, eight-wheel steer, scaled electric combat vehicle (SECV). The SECV prototype is capable of assigning an independent wheel speed as well as an independent steering angle to any of its eight wheels and will be used as a tool for future autonomous research. The vehicle was initially constructed at Ontario Tech University and is fully electric with independent motors for each wheel allowing for independent eight wheel drive as well as eight wheel steering [13]. The vehicle is presented in Figure 1.

Figure 1 Side View of 8x8 SECV [14]

II. THEORETICAL VEHICLE MODEL

A. Ackermann Steering Relationship

As stated earlier the 8x8 SECV has implemented the full Ackermann steering condition for its control. In terms of steering, the Ackermann condition assigns a unique steering angle to each steerable wheel during a turn. Specifically, for a right and left turn wheels are denoted as inner or outer wheels. For example, for a right turn: the wheels on the right side of the vehicle are inner wheels (i) and the wheels on the left side are the outer (o) wheels. According to the Ackermann condition, wheels during a turn must trace circles of different radii meaning the inner wheel must be steered at a sharper angle. In this way all wheels have their axles placed on the radii of circles that share a common center point. Using the Ackermann relationship, three steering configurations are implemented on the physical vehicle: traditional (front two axle steering), fixed third axle steering (axle 1, 2 and 4 steering) and all wheel steering.

The focus of this investigation will involve the third steering configuration: the all-wheel steering configuration, however the other two configurations have been modelled and validated.

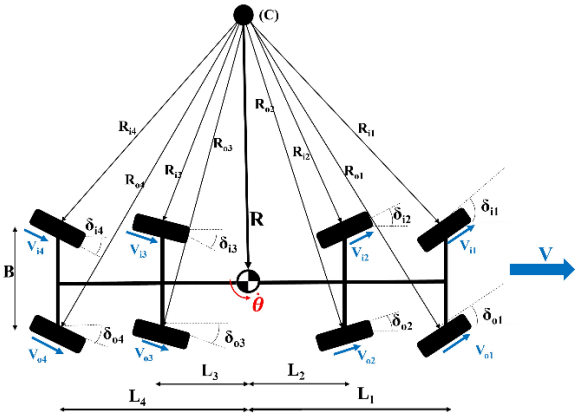

Figure 2 Ackermann All Wheel Steering Configuration

Figure 2 shows the all-wheel steering configuration applying a steering angle according to the Ackermann condition to all eight wheels. All parameters are explained in proceeding sections.

B. SECV Hardware and Specifications

As stated earlier, the SECV is capable of actuated steering for all eight of its wheels as well as capable of varying the speed of all eight of its wheels in real time. Detailed specifications of the vehicle are seen in Table I and Table II. The values for the wheelbase lengths for each steering configuration are seen in Table I.

TABLE I. WHEELBASE VALUES FOR EACH STEERING CONFIGURATION

Wheelbase Lengths (L)	
Ackermann All Wheel Steering	***Values (meters)***
L_1	0.3022
L_2	0.0989
L_3	0.0989
L_4	0.3022

Other general parameters that signify key components or dimensions in the SECV are seen in Table II.

TABLE II. GENERAL PARAMETERS OF SECV

General Parameters	
Parameter	***Value[a]***
Trackwidth (B)	0.465m for all axles
Chassis Length	1.124 (m)
Chassis Width	0.606 (m)
Chassis Height	0.596.3 (m)
Max Speed	1.6(m/s)
Total Mass	45(kg)
Suspension Rating	30(lb) gas shock absorbers & 10(lb) coils (quantity: 8)
Steering Hardware	12(V) P16 Linear Actuators (quantity: 8)
Driving Hardware	15(V) Brushed Motor (quantity: 8)

a. The units are m – meters, V – Volts, lbf – Pound force, s – second, kg - kilograms.

The main hardware components and their connections are presented in Figure 3. The two separate signals for steering and driving are sent to the main controller board. The steering input is split between two sub-controllers which are responsible for the linear actuator extension to perform the actuated steering for the front and rear axle's wheels respectively. The linear actuator is composed of a potentiometer sensor to ensure accurate travel of the actuators, and this results in an error of 0.3mm for 50mm of travel. The driving input is sent through the main controller to all four motor controllers. Each motor controller controls two motors and performs the driving for the wheels on one axle. In addition, the shaft of each motor is connected to an encoder which is connected in a feedback loop back to the respective motor controller. The encoder and motor controller feedback connection ensure the correct wheel speed in RPM is provided to the motor and transferred correctly to the wheels through the drivetrain.

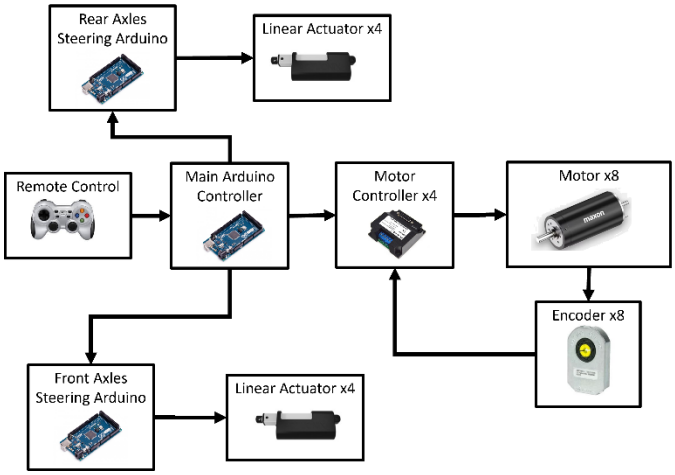

Figure 3 8x8 SECV Hardware Block Diagram

III. STEERING METHODOLOGY

A. Actuator Stroke Distance and Wheel Angle Relationship

Prior to leveraging the Ackermann control method, low level control relating the actuator extension to steering wheel actuation angle is performed. It is seen that the actuator extends linearly, pushing out the wheel to develop an angle on the wheel being steered. This is exemplified in Equation 1.

$$l = r_t \theta_t \tag{1}$$

The steering angle applied to a wheel is created using a linear actuator to push the wheel as it travels. Where (r_t) represents the tire radius for the SECV. The true tire radius is 3.675 inches or 93.3mm. The steering rod does not connect exactly on the perimeter of the tire. Therefore, the smaller value of 2.8 inches or 71.1mm is used. The actuator stroke distance (l) has a standard operable range from 0 to 45mm with an absolute maximum extension of 50mm. (θ_t) is the developed angle on the wheel. Equation 1 is used to select the first wheel inner steering angle which will have the largest angle. This is applied to the vehicle through remote control.

B. Vehicle Turning Radius

Equation 2 defines the minimum turning radius for the vehicle given a selected inner wheel's steering angle. The turning radius (R) is the shortest distance in the lateral direction from the common center point for a given steering configuration, seen in Figure 2.

$$R = \frac{L_1}{\tan(\delta_{ij})} + \frac{B}{2} \tag{2}$$

For the all-wheel steering configuration this is the geometric centre of the vehicle and the centre point (C) of the turn. Due to the mechanical limits of the steering linkages the maximum steering range for the first axle inner wheel angle is seen to be: (-20) degrees to (+20) degrees. This is also the maximum steering angle actuation for all of the eight wheels. The turning radius is found according to Equation 2, given the selected first axle inner wheel steering angle (δ_{i1}). Using the Equation 2 relationship and the correct wheelbase value (L_1) the current turning radius is calculated. Following this, the remaining 7 wheels' steering angles are calculated with each wheel being denoted as an inner or outer wheel depending on their positioning with regards to the left or right turn.

C. Steered Wheel Angle

Using the previously found turning radius (R), the vehicle trackwidth (B) and the correct wheelbase value the inner and outer wheel angles are found. Equation 3 and 4 are similar except that there is a summation in Equation 3 for inner wheel angles and a subtraction in Equation 4 for outer wheel angles.

1) Inner Wheel of Turn Angle

$$\delta_{ij} = \tan^{-1}\left(\frac{L_j}{R - \frac{B}{2}}\right) \tag{3}$$

2) Outer Wheel of Turn Angle

$$\delta_{oj} = \tan^{-1}\left(\frac{L_j}{R + \frac{B}{2}}\right) \tag{4}$$

IV. DRIVING METHODOLOGY

A. Variable Wheel Speed Control

The SECV is capable of varying the speed of its wheels independent of one another. In other words, each wheel can be assigned a unique velocity, allowing the SECV to be driven with all eight wheels spun at eight different rates. The following equations shown in more detail explain the relationship between the different velocities of each wheel according to the Ackermann condition. By varying the speed of different wheels in this way the vehicle can achieve the Ackermann condition at low speeds and greatly reduce tire scrubbing as the wheels trace out independent radii during a turn. Wheels located on the outside of the turn will have a higher velocity allowing for a sharper turn. In addition, wheels on one side, with respect to a turn (inside or outside of the turn) will vary according to the Ackermann condition as shown in the results in the proceeding sections of this paper.

B. Individual Wheel Turning Radius

In order to calculate the ideal wheel velocity to navigate the turn according to the Ackermann condition a turning radius for each wheel is required. This is seen in Equation 5 for inner wheels' radius (R_{ij}) and Equation 6 for outer wheels' radius (R_{oj}) respectively. This wheel turning radius is the radius of the circular path traced out by a specific wheel for a specific steering angle (δ_{ij}) and (δ_{oj}).

$$R_{ij} = \frac{L_j}{sin\delta_{ij}} \tag{5}$$

$$R_{oj} = \frac{L_j}{sin\delta_{oj}} \tag{6}$$

C. Yaw Rate

A centerline longitudinal velocity (V) is transmitted to the vehicle. During experimentation as seen in proceeding sections of this paper, a longitudinal velocity of 2km/h is used. The yaw rate is found using the longitudinal velocity and the turn radius of the vehicle (R). The yaw rate represents the rate of change of heading of the vehicle. This is seen in Equation 7.

$$\dot{\theta} = \frac{V}{R} \tag{7}$$

D. Individal Wheel Velocity

As seen in the differing steering configurations, certain axles have their wheels fixed, while others are steerable (traditional steers only first two axles' wheels, fixed third axle steers the wheels on all axles except axle 3, while the all-wheel steering configuration steers the wheels on all four axles). However, although certain wheels are not steered, all wheels are powered for driving and no wheels are free spinning. In other words, all eight wheels and their connected motors provide torque and are required for the full tractive effort of the vehicle. For the purposes of this investigation only the Ackermann All-wheel results are presented meaning all wheels are steerable. Results for the other two configurations that leverage non-steerable wheels can be provided upon request.

1) Wheel Velocity of steerable wheels

Wheels that are steerable vary their speed according to the Ackerman condition equations. Equation 8 and Equation 9 leverage the steerable wheels' individual wheel turning radii (R_{ij} and R_{oj}) as well the yaw rate to find the velocity of the steerable wheels for inner (V_{ijs}) and outer (V_{ojs}) wheels respectively. For the all-wheel steering configuration these equations will be used to find wheel speed as all wheels are steerable in this case.

$$V_{ijs} = \dot{\theta} R_{ij} \tag{8}$$

$$V_{0js} = \dot{\theta} R_{oj} \tag{9}$$

2) Wheel Velocity of non-steerable wheels

Wheels that are fixed continue to vary their speed linearly according to remote control input and do not leverage the Ackermann condition and individual wheel turning radii (R_{ij} and R_{oj}) for their wheel speeds. The velocity of fixed, non-steerable wheels for inner (V_{ijf}) and outer (V_{ojf}) is seen in Equation 10 and Equation 11 respectively and leverages the turning radius of the vehicle (R), track width (B) and yaw rate.

$$V_{ijf} = \dot{\theta}\left(R - \frac{B}{2}\right) \tag{10}$$

$$V_{ojf} = \dot{\theta}\left(R + \frac{B}{2}\right) \tag{11}$$

V. Steering Analysis Results

Using the remote-control input, a steering angle is sent to the first axle inner wheel of the turn. This is the largest steering angle developed out of all eight wheels. Using this angle (δ_{i1}), the angles of the remaining seven wheels are calculated using Equation 1 to 4 seen previously. The vehicle is evaluated while stationary on a raised stand to verify the output steering angles on the wheels.

A. Experimental Methodology

The theoretical results are developed using the previous equations. However, validation is required to ensure the output wheel angles based on the theoretical design are accurate. To verify the correct values, the output wheel extensions recorded by the potentiometer in the linear actuators are captured in real time. Putty serial connection software is used alongside the Arduino controller to perform this task. These extensions are converted to the corresponding wheel angles. The maximum steering angle possible for the 8x8 SECV on any wheel is ±20 degrees. This angle results in an actuator extension of 49mm, with the max operable extension of each actuator being 50mm. In normal operation while driving the max angle is set to ±18 degrees to preserve the life of the linear actuators. The error present on each linear actuator is 0.3mm.

B. Ackermann All-Wheel Steering – Wheel Angles

The all-wheel steering configuration involves the complete Ackermann condition implemented on the 8x8 SECV for all eight wheels. As seen in Figure 2, because all eight wheels are steered, the instantaneous centre (C) is located in the geometric centre of the vehicle. The steering angles of all eight wheels are graphed and presented in Figure 4.

1) Theoretical Results

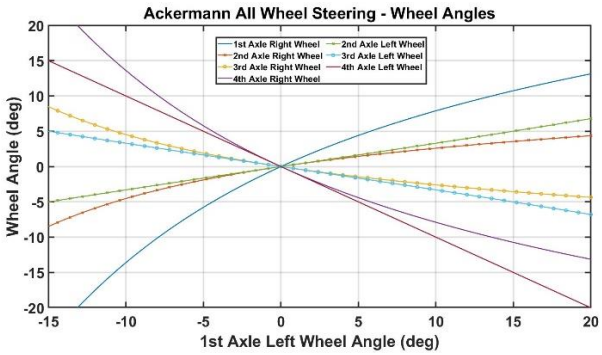

Figure 4 All Wheel Steering Configuration: Theoretical Wheel Angles

The all-wheel steering configuration actuates all eight wheels according to the Ackermann equation. In this case, it is seen that the first axle right wheel has the largest range of steering angles from (-40º) to (12º) and that the fourth axle right wheel is symmetric having the same range of steering angles but reversed, ((40º) to (-12º)). This same pattern exists between the right wheels of the second and third axle with these wheels

sharing the same symmetry. This symmetry exists due to the geometry of the vehicle and identical track width between all axles.

2) Experimental Results

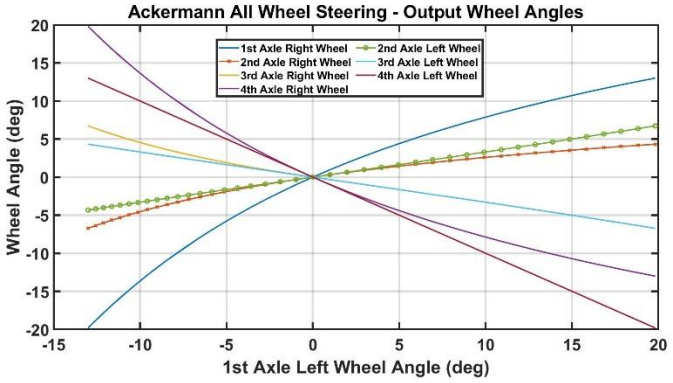

Figure 5 Ackermann All Wheel Steering Experimental Output Wheel Angles

The experimental output wheel angles are shown for the All-wheel steering configuration in Figure 5. The maximum allowable angle on a wheel due to the steering linkages and mechanical components of the vehicle is 20 degrees. The linear actuator output extensions are collected, and the resultant wheel angles are found using Equation 1 by relating the actuator extension to the wheel angle and tire radius. It is seen that when the first axle left wheel has a negative angle the vehicle is conducting a right turn. Thus, the first axle left wheel is no longer the inner wheel and therefore no longer has the maximum steering angle. Overall, the actuator extensions are quite accurate due to the linear actuators' potentiometer providing feedback and thus clearly match the theoretical results. The experimental results have minimal error compared with the theoretical wheel angles with the profiles being almost identical.

VI. Velocity Analysis Results

Initially, a longitudinal velocity (V) is applied along the centreline of the vehicle. After steering angles are generated, an individual wheel turning radius is found for each inner (R_{ij}) and outer (R_{oj}). The longitudinal velocity (V) is used alongside the vehicle's minimum turning radius (R) to find the yaw rate. Furthermore, given a predetermined longitudinal speed (for all experiments 2km/h is used) wheels that are steerable calculate their wheel speed according to the individual wheel turning radii as seen in previous equations for inner wheels (V_{ijs}) and for outer wheels (V_{ojs}). Similarly wheels that are not steerable do not develop a steering angle and as such have no wheel turning radius. As such, the vehicle's minimum turning radius is used in this case to calculate the wheel speeds for these fixed-steering wheels according to the previous equations for inner (V_{ijf}) and outer (V_{ojf}) wheels respectively.

A. Experimental Methodology

In order to verify and validate the wheel speeds, the output wheels speeds are measured. A handheld tachometer is used to record the rotations per minute (RPM). The tachometer has an average error of ±2 RPM. The effect of this tachometer error is more pronounced at lower speeds, particularly speeds below 1km/h. Overall, at a speed of 2km/h wheel speed values in RPM are seen to be between 70RPM and 90RPM. This results in a maximum error of 3% when using the tachometer. Using the tire and the RPM found through the tachometer the wheel speed in km/h is found for all wheels.

B. Ackermann All-Wheel Steering – Wheel Speeds

The all-wheel steering configuration is the complete Ackermann condition implemented on the 8x8 SECV for all eight wheels and all wheels are steerable. As such all eight wheels are following Equation 8 and Equation 9 to develop their wheel speeds. It is seen that the minimum turning radius of the 8x8 SECV when using the Ackermann all wheel steering configuration is the lowest with a value of 0.9m. In short, all eight wheels are contributing the steering effort.

1) Theoretical Results

The turning radius for the vehicle is reduced by 53 % compared with the Traditional steering configuration and reduced by 48% when compared with the fixed third axle steering configuration. In Figure 6, it is also seen that the velocity profiles for certain wheels overlap. This is due to the symmetry of the vehicle and the centre of the vehicle turning radius overlapping with the geometric centre of the vehicle.

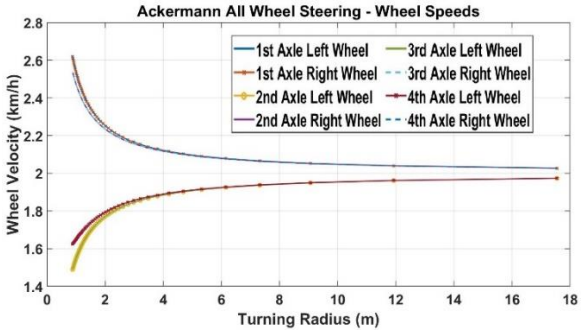

Figure 6 All Wheel Steering Configuration: Wheel Speeds

It is seen that the right-side wheels for the first and fourth share the same velocity profile and the second and third wheels share the same profile. The same is true for the other side. The graph shows that the Ackermann all wheel steering configuration provides the absolute minimum turning radius of 0.9m for the vehicle.

1) Experimental Results

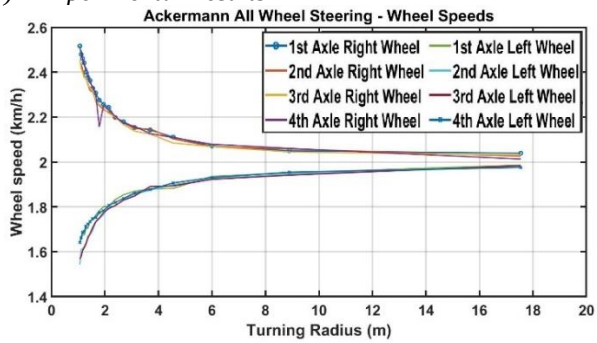

Figure 7 Ackermann Steering Configuration: Output Wheel Speeds

As seen in Figure 7, the output wheel speeds for the Ackermann steering configuration are presented. The physical

experimentation for the Ackermann steering configuration had the least error overall and best matched the theoretical results. This can be credited to this configuration requiring the highest speed differential on the 8x8 SECV during a turn. The deviations in this graph are attributed to the miniscule 3% error of the tachometer. Overall, the profile of the graph matches near identically to the theoretical results.

VII. Conclusion

This research paper is focused on the physical experimentation and validation of the wheel speed and steering control of an eight-wheel drive and eight-wheel steering vehicle: The 8x8 SECV. The control algorithm is based in the Ackermann condition which involves assigning individual steering angles to each wheel so that they may trace a circular path during a turn that results in minimal lateral tire scrubbing. In total, three separate steering configurations are designed and implemented: Traditional (front two axle's wheels are steering), fixed third axle steering (wheels on axles 1,2 and 4 are steerable) and Ackermann All wheel steering (all four axle's wheels are steerable). The main benefit of using these configurations is to minimize the tire wear associated with lateral tire scrubbing. The steering configurations are implemented alongside the steering actuators, driving motors and associated controllers. The vehicle is tested while stationary on a raised platform to better visualize the steering angles and varying wheel speeds between wheels.

Initially the theoretical results are presented showing the numerical model for the control of the wheel speeds and steering. The results showed that the all-wheel steering configuration has a reduction of 53% in vehicle turning radius compared with the traditional steering configuration and a 48% reduction in turning radius compared with the fixed third axle steering configuration.

Physical validation through experimentation was also performed. The output steering angles developed by all wheels was measured and collected. It is noted that 20 degrees is the maximum allowable steering angle for a wheel due to the mechanical components and steering linkages. This accurate steering performance can be credited to the linear actuator potentiometer performing feedback control of the actuator to ensure at most the developed error will be 0.3mm for 50mm of actuation.

The output wheel speeds for all steering configurations are also validated using a handheld tachometer to record the wheel speeds at each degree of steering as a wheel is steering through 20 degrees of steering. A right turn is used as the procedure for this experiment. The output wheel speeds graphs of all steering configurations closely matched the theoretical results.

Future developments will involve implementing the various steering configurations alongside an autonomous navigation system. A major benefit of this implementation is allowing the vehicle to decide which steering configuration to leverage based on the environmental conditions. Currently autonomous vehicle platforms are being used for a wide range of research, however many of these platforms lack car-like features such as suspension and actuated steering. This future work will also involve one of the first physical implementations of varied steering configurations and their effect on autonomous navigation performance.

Acknowledgment

The authors would like to express their gratitude to the Natural Sciences and Engineering Research Council of Canada (NSERC Discovery Grant) for their continuous support during this study.

References

[1] M. Park, S. Lee, M. Kim, J. Lee, and K. Yi, "Integrated differential braking and electric power steering control for advanced lane-change assist systems," Proceedings of the Institution of Mechanical Engineers, Part D: Journal of Automobile Engineering, vol. 229, no. 7, pp. 924-943, 2015.

[1] M. Park, S. Lee, M. Kim, J. Lee, and K. Yi, "Integrated differential braking and electric power steering control for advanced lane-change assist systems," *Proceedings of the Institution of Mechanical Engineers, Part D: Journal of Automobile Engineering*, vol. 229, no. 7, pp. 924-943, 2015.

[2] Y. Ye, L. He, and Q. Zhang, "Steering Control Strategies for a Four-Wheel-Independent-Steering Bin Managing Robot," *IFAC-PapersOnLine*, vol. 49, no. 16, pp. 39-44, 2016/01/01/ 2016.

[3] M. Peiris, M. El-Gindy, and H. Lang, "Filtering based sensor fusion positioning methods: literature review," *International Journal of Vehicle Systems Modelling and Testing*, vol. 17, pp. 311-325, 01/01 2023.

[4] S. Wei, Y. Zou, X. Zhang, T. Zhang, and X. Li, "An Integrated Longitudinal and Lateral Vehicle Following Control System With Radar and Vehicle-to-Vehicle Communication," *IEEE transactions on vehicular technology*, vol. 68, no. 2, pp. 1116-1127, 2019.

[5] B. Lenzo, M. Zanchetta, A. Sorniotti, P. Gruber, and W. De Nijs, "Yaw Rate and Sideslip Angle Control Through Single Input Single Output Direct Yaw Moment Control," *IEEE transactions on control systems technology*, vol. 29, no. 1, pp. 1-16, 2020.

[6] W. Lee, H. Cho, S. Hyeong, and W. Chung, "Practical modeling of GNSS for autonomous vehicles in urban environments," *Sensors (Basel, Switzerland)*, vol. 19, no. 19, p. 4236, 2019.

[7] N. De Raeve, M. de Schepper, J. Verhaevert, P. Van Torre, and H. Rogier, "A Bluetooth-Low-Energy-Based Detection and Warning System for Vulnerable Road Users in the Blind Spot of Vehicles," *Sensors (Basel, Switzerland)*, vol. 20, no. 9, p. 2727, 2020.

[8] J. Liang, U. Patel, A. J. Sathyamoorthy, and D. Manocha, "Realtime Collision Avoidance for Mobile Robots in Dense Crowds using Implicit Multi-sensor Fusion and Deep Reinforcement Learning," *arXiv.org*, 2020.

[9] S. Papatheodorou, A. Tzes, K. Giannousakis, and Y. Stergiopoulos, "Distributed area coverage control with imprecise robot localization: Simulation and experimental studies," *International journal of advanced robotic systems*, vol. 15, no. 5, p. 172988141879749, 2018.

[10] M. Ahmed, M. El-Gindy, and H. Lang, "Path-following enhancement of an 8 × 8 combat vehicle using active rear axles steering strategies," *Proceedings of the Institution of Mechanical Engineers. Part K, Journal of multi-body dynamics*, vol. 235, no. 4, pp. 539-552, 2021.

[11] M. Ahmed, M. El-Gindy, and H. Lang, "A novel genetic-programming based differential braking controller for an 8×8 combat vehicle," *International journal of dynamics and control*, vol. 8, no. 4, pp. 1102-1116, 2020.

[12] M. Ahmed, M. Omar, and M. El-Gindy, "Investigation of various passive steering modes for a multi-wheeled combat vehicle," *International Journal of Vehicle Systems Modelling and Testing*, vol. 15, no. 2-3, pp. 188-203, 2021/01/01 2021.

[13] A. H. Tan, M. Peiris, M. El-Gindy, and H. Lang, "Design and development of a novel autonomous scaled multiwheeled vehicle," *Robotica*, vol. 40, no. 5, pp. 1475-1500, 2022.

[14] J. Tse, M. Peiris, M. El-Gindy, and Z. El-Sayegh, "Control Architecture Development of an 8x8 Scaled Electric Combat Vehicle," in *Canadian Society of Mechanical Engineers*, Edmonton, Alberta, Canada, 2022, vol. 5: CSME 2022 Proceedings.